AD-A067 665 NAVAL RESEARCH LAB WASHINGTON D C F/G 4/2
FEASIBILITY OF SHIPBOARD LASER-ATTENUATION MEASUREMENTS WITH A --ETC(U)
FEB 79 H GERBER
UNCLASSIFIED NRL-8290 SBIE-AD-E000 286 NL

| OF |
AD
A067665

END
DATE
FILMED
6-79
DDC

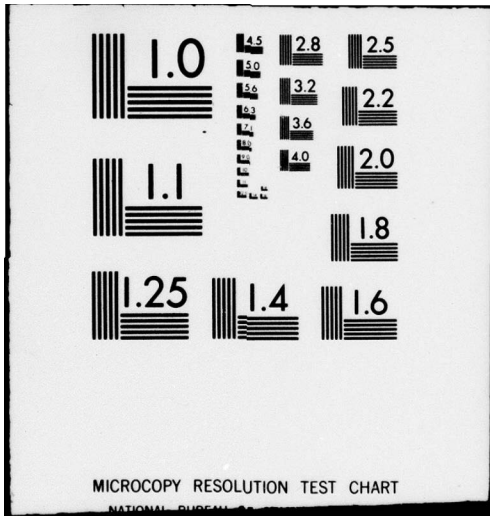
1.0
1.1
1.25
1.4
1.6
1.8
2.0
2.2
2.5
2.8
3.2
3.6
4.0
4.5
5.0
5.6
6.3
7.1
MICROCOPY RESOLUTION TEST CHART

(12) LEVEL III

NRL Report 8290

Feasibility of Shipboard Laser-Attenuation Measurements With a Portable Transmissometer

H. GERBER

Atmospheric Physics Branch
Ocean Sciences Division

February 26, 1979

NAVAL RESEARCH LABORATORY
Washington, D.C.

SECURITY CLASSIFICATION OF THIS PAGE *(When Data Entered)*

REPORT DOCUMENTATION PAGE

READ INSTRUCTIONS BEFORE COMPLETING FORM

1. REPORT NUMBER: NRL Report 8290
2. GOVT ACCESSION NO.:
3. RECIPIENT'S CATALOG NUMBER:

4. TITLE *(and Subtitle)*: FEASIBILITY OF SHIPBOARD LASER-ATTENUATION MEASUREMENTS WITH A PORTABLE TRANSMISSOMETER

5. TYPE OF REPORT & PERIOD COVERED: Interim report on the NRL Problem

6. PERFORMING ORG. REPORT NUMBER:

7. AUTHOR(s): H. Gerber

8. CONTRACT OR GRANT NUMBER(s): 62759N

9. PERFORMING ORGANIZATION NAME AND ADDRESS: Naval Research Laboratory, Washington, DC 20375

10. PROGRAM ELEMENT, PROJECT, TASK AREA & WORK UNIT NUMBERS: NRL Problem A03-14B, Project WF52-551-715

11. CONTROLLING OFFICE NAME AND ADDRESS: Department of the Navy, Naval Air Systems Command, Washington, DC 20361

12. REPORT DATE: February 26, 1979

13. NUMBER OF PAGES: 21

14. MONITORING AGENCY NAME & ADDRESS *(if different from Controlling Office)*: Department of the Navy, Naval Ocean Systems Center, San Diego, CA 92152

15. SECURITY CLASS. *(of this report)*: UNCLASSIFIED

15a. DECLASSIFICATION/DOWNGRADING SCHEDULE:

16. DISTRIBUTION STATEMENT *(of this Report)*

Approved for public release; distribution unlimited.

17. DISTRIBUTION STATEMENT *(of the abstract entered in Block 20, if different from Report)*

18. SUPPLEMENTARY NOTES

19. KEY WORDS *(Continue on reverse side if necessary and identify by block number)*

Portable transmissometer
Integrating nephelometer
Transmission measurements
Aerosol extinction
Aerosol scattering
Aerosol absorption
Refractive index of particles
Concentrated aerosol particles

20. ABSTRACT *(Continue on reverse side if necessary and identify by block number)*

A 2-meter-long cell has been devised in which aerosol extinction and scattering coefficients can be measured simultaneously. Extinction is obtained by measuring the change in the intensity of a HeNe laser beam which is stepped through the cell for a total path length of 20 meters. A reciprocal nephelometer consisting of a sensor with a precise Lambertian response is mounted on the side of the cell to give a direct measure of the scattering coefficient. Filling the cell with ambient aerosol that has been concentrated centrifugally increases the effective path length of the beam in the cell to 300 meters.

(over)

DD FORM 1 JAN 73 1473 EDITION OF 1 NOV 65 IS OBSOLETE
S/N 0102-014-6601

SECURITY CLASSIFICATION OF THIS PAGE *(When Data Entered)*

20. Abstract (Continued)

The cell was taken on the 1977 EOMET cruise of the USNS *Hayes* in order to determine its capabilities when exposed to the rigors of a ship's environment. The variance of data collected during the cruise was analyzed. The mean resolution limit of the transmittance measurements made during the cruise was ± 0.16 percent. This limit was primarily influenced by mechanical instabilities in the cell, which were greatest during rough seas, and large ambient-cell-temperature differences. The nephelometer operated precisely. Vibrations from the ship's machinery was damped out successfully. An improved cell could increase the resolution by a factor of 10 or more. Absorption coefficients of the aerosol particles in the eastern North Atlantic and in the Mediterranean were plotted. This technique has potential in the infrared.

+ or - 0.16%.

CONTENTS

FEASIBILITY OF SHIPBOARD LASER-ATTENUATION MEASUREMENTS WITH A PORTABLE TRANSMISSOMETER

INTRODUCTION

Transmittance measurements in the marine environment are scarce, since ships, which are the most convenient measurement platform, cannot accommodate the required baseline, which is on the order of 1 km [1]. A new transmissometer was developed which no longer requires a 1-km baseline. It consists of a cell only 2 meters long, thus giving it portability. The reduction in size was permitted by finding means of making transmittance measurements which were at least an order of magnitude better than measurements by other systems. Tests of the new transmissometer with laboratory aerosol showed accuracies of 0.1% in transmittance measurements. This extraordinary accuracy is due to the following features of the system:

- Fluctuations in light source intensity and receiver sensitivity become unimportant by illuminating the *same* receiver with phase shifted pulses of the transmitted and the reference light beam;

- The influence of the optics which step the beam through the transmission cell are subtracted by *cycling* clean air and aerosol through the chamber;

- The signal-to-noise ratio of the transmittance measurement is increased by filling the chamber with concentrated aerosol [2].

The portable transmission cell was aboard the USNS *Hayes* for the duration of the 1977 EOMET cruise (Fig. 1). The goal of this effort was to determine the feasibility of using the portable system in a shipboard environment. Answers to the following questions were sought: How do the ship's vibrations and wave-induced motions influence the accuracy of the transmittance measurements? Is the measurement through the aerosol concentrate in the cell compatible with the actual atmospheric transmittance? Given favorable answers to the preceding questions, how applicable is the system for transmittance measurements in the infrared?

Manuscript submitted October 11, 1978.

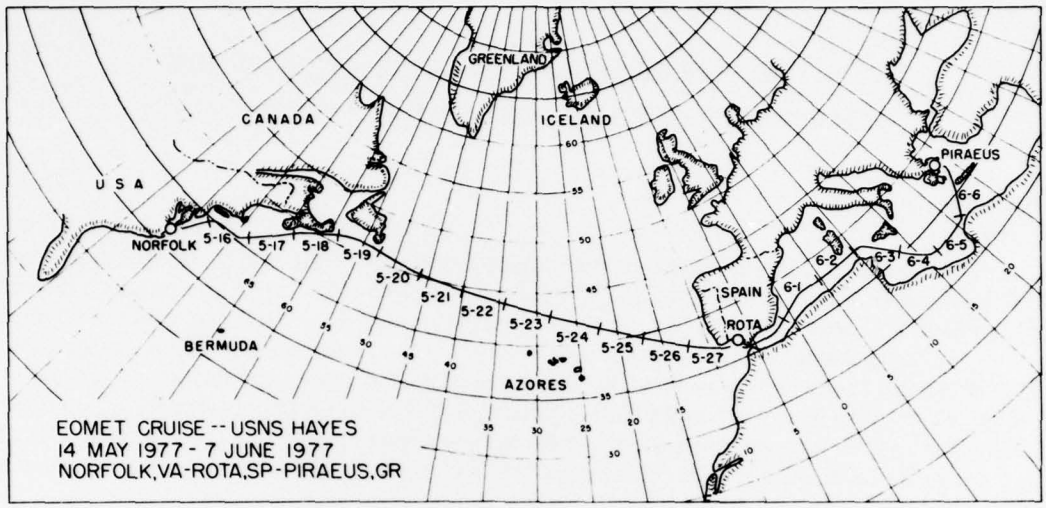

Fig. 1 — Track of the USNS *Hayes* during the 1977 electrooptics meteorology (EOMET) cruise

The cell was instrumented with a HeNe laser operating at 632.8 nm. The usefulness of this wavelength for data accumulation in a marine environment is small, since existing nephelometers (such as described by Charlson et al. [3]) give similar data, provided that the measurements are not made in an urban atmosphere where absorption plays a large role [4] and that a correction for the wavelength of light is made. The real usefulness of the portable transmissometer would be for wavelengths in the infrared, for which wavelengths no nephelometers exist and standard transmissometer measurements are error prone. However, the cost factor and the simplicity of a HeNe laser and associated optics were the deciding factors in using this wavelength to test the feasibility of this approach. The cell was also instrumented with a reciprocal form of the standard nephelometer [5]. This addition made it possible to measure the extinction and scattering in the same volume of aerosol, thus permitting in-situ measurements of the absorption coefficient of the particles. The nephelometer also provided the evidence needed to judge the optical quality of the concentrated aerosol in the cell.

THEORETICAL ASPECTS

Aerosol Extinction

The transmittance of monochromatic, single-scattered light through aerosol is given by the Bouguer-Beer law,

$$\frac{I}{I_0} = e^{-\tau}, \tag{1}$$

where I_0 is the incident intensity and I is the transmitted intensity of a light beam passing through a slab with optical depth τ, where

$$\tau = (b_s + b_a + m_s + m_a)\, x ,$$

in which b_s and b_a are the scattering and absorption coefficients respectively for the aerosol, m_s and m_a are the scattering and absorption coefficients for the air molecules, and x is the slab thickness.

Equation (1) does not apply to measurements through the portable cell unless reflection losses due to mirrors are accounted for, since the laser beam follows a folded path to the receiver. Given that these losses have a total fractional value L, Eq. (1) becomes

$$\frac{I}{I_0} = Le^{-\tau} .$$

During calibration the cell is filled with particle-free air, which gives $\tau \approx 0.0$, since $m_s + m_a \approx 0.0$ for the visible laser wavelength and the short baseline used. The second step is to decrease the intensity of the reference beam by the factor L, so that during calibration $I/I_0 = 1.0$ and during measurements Eq. (1) is valid.

Also, Eq. (1) does not apply unless a negligible amount of single- and multiple-scattered light from the particles enters the receiver, since otherwise the transmittance is erroneously overestimated. Zuev et al. [6] have shown that for collimated light beams the scattered component is unimportant for $\tau \leqslant 25$ as long as the divergence of the light beam and aperture of the receiver are less than about 3 mrad (0.17 deg). Since the optics of the cell meet those requirements, the cell can measure atmospheric visibilities as low as about 150 m, which value is obtained by using the preceding value of τ with Koschmieder's formula.

Rather than give the transmittance, the electronic processing of the receiver output gives the extinction of light due to the particles which is simply

$$\frac{\Delta I}{I_0} = 1 - \frac{I}{I_0} = 1 - e^{-(b_s + b_a)\, x} , \tag{2}$$

with m_s and m_a again being neglected.

Aerosol Scattering

The flux F of light scattered by particles illuminated by a narrow collimated beam into a sensor with a cosine response and area S is given by

$$F = \frac{b_s I_0 S}{2\pi h} , \tag{3}$$

where h is the perpendicular distance between the sensor and the collimated beam [7].

For the present cell I_0 is not constant due to the loss of light intensity at each reflection off the parallel mirrors, and h also changes as the beam steps away from the cosine sensor (Fig. 2). To reflect this behavior, Eq. (3) is changed to

$$F = \frac{b_s S}{2\pi}\left(\frac{I_1 + I_2}{2h_1} + \frac{I_3 + I_4}{2h_2} + \ldots + \frac{I_{19} + I_{20}}{2h_{10}}\right) , \tag{4}$$

where $I_0 = I_1$. Each term in Eq. (4) consists of the arithmetic mean of the intensities at the extremes of each leg; this was found to be sufficiently accurate, even though the intensity changes exponentially in each leg and some contribution to F comes from the virtual images of the beam for large h. The mirror reflections occur following each even-numbered intensity except for I_{20}. The intensities in each leg are related by the use of the exponential-attenuation law (Eq. (1)), from which

$$\frac{I_{i+1}}{I_i} = \left[e^{-bx(i+1)/2}\right] , \quad i = 1, 3, 5, \ldots, 19, \tag{5}$$

where the extinction coefficient b is equivalent to $b_s + b_a$.

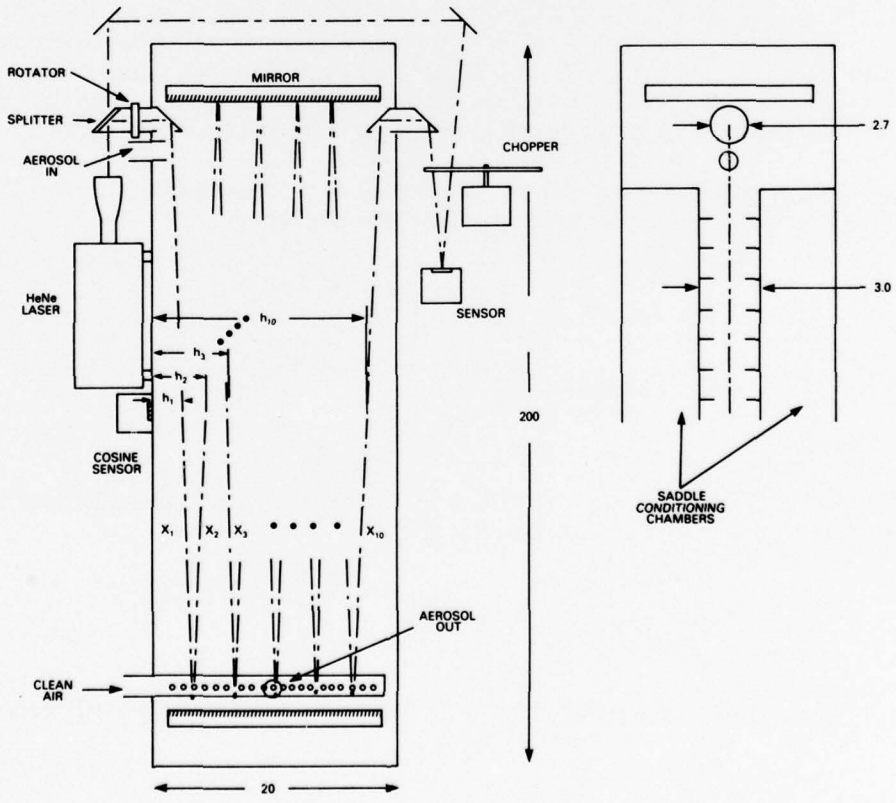

Fig. 2 — Schematic of the transmission cell showing the laser-beam path, location of the optics, and dimensions (cm)

Calibration of the cosine sensor consists of filling the cell with Freon 12, which has a known molecular scattering coefficient b_{sc} at the 6328-nm wavelength [8]. Since the Freon 12 attenuates the laser beam in the ≈20-m pathlength by less than 0.5%, it can be assumed that

$$I_i = I_{i+1}, \quad i = 1, 3, 5, \ldots, 19; \tag{6}$$

and since

$$I_{i+1} = I_i R, \quad i = 2, 4, 6, \ldots, 18, \tag{7}$$

where R is the reflectivity of the mirrors, the calibration flux F_c found from Eq. (4) is

$$F_c = \frac{b_{sc} S I_1}{2\pi} \sum_{i=1}^{10} \frac{R^{i-1}}{h_i}. \tag{8}$$

Combining Eqs. (4), (5), (7), and (8) gives the flux seen by the cosine sensor in the cell filled with aerosol:

$$F = \frac{b_s F_c \sum_{i=1}^{10} \frac{R^{i-1}}{h_i} \left[\exp\left(-b \sum_{j=0}^{i-1} x_j\right)\right] \left(1 + e^{-bx_i}\right)}{2 b_{sc} \sum_{i=1}^{10} \frac{R^{i-1}}{h_i}}, \tag{9}$$

where $x_0 = 0$ and angular truncation losses have been neglected. Equations (2) and (9) are solved for the two unknown quantities b_s and b_a.

Particle-Size Bandpass

The lower size limit of the particle bandpass in the aerosol concentrator occurs when particles are drawn into the porous cylindrical rotor (Fig. 3) and become part of the volume flow rate V_3 of the dispersion medium being removed instead of the volume flow rate V_2 of the aerosol concentrate. This occurs when the particles' Stokes velocity due to the centrifugal field created by the spinning rotor is less than the mean suction velocity into the rotor. Thus the size limit is found by equating those two velocities:

$$\frac{D^2 \rho \omega^2 R_1}{18\eta} \left[1 + \frac{2\lambda}{D}\left(A + Be^{-CD/2\lambda}\right)\right] = \frac{V_1 - V_2}{2\pi R_1 L}, \tag{10}$$

where D is the diameter of a spherical particle with density ρ, R_1 is the radius of the rotor, L is the length of the rotor, ω is the angular velocity of the rotor, V_1 is the flow rate into the concentrator, V_2 is the concentrate flow rate, λ is the mean free path of air, η is the viscosity of air, and A, B, and C are slip corrections usually assigned the values 1.246, 0.42, and 0.87 respectively.

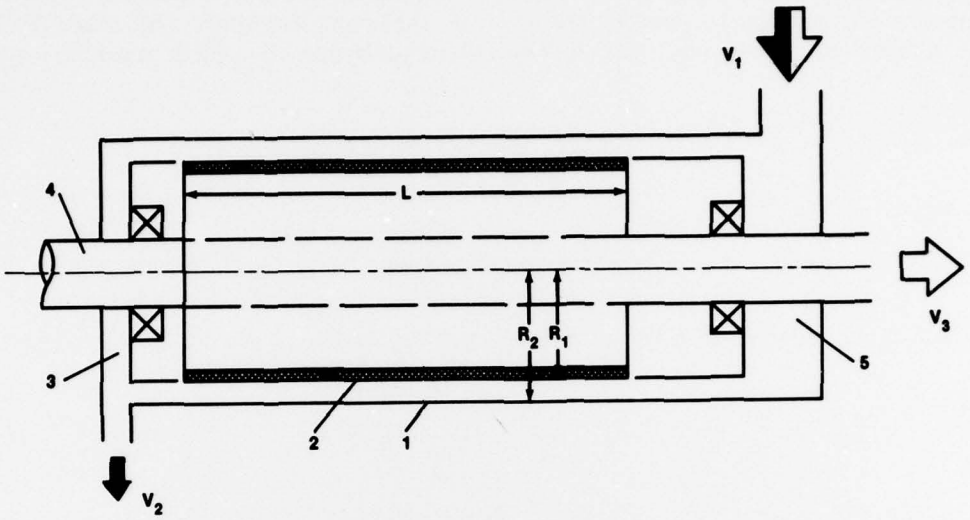

Fig. 3 — Schematic of the aerosol concentrator

The upper size limit is difficult to determine theoretically, since it is partially a result of turbulent impaction losses. However, a best case can be calculated for "stirred settling" losses [9] in a chamber of size R_1 and L.

Filling Rate of the Cell

The time dependence of particle concentration $C(t)$ in the cell which, after being flushed with filtered air and filled with aerosol concentrate, is given by

$$\frac{C(t)}{C} = \frac{V_1}{V_2} \; 1 - e^{-tV_2/V} \quad , \tag{11}$$

where C is the particle concentration in the concentrate, t is time, and V is the volume of the cell.

INSTRUMENTATION

Geometry of the Cell

The transmission cell (Fig. 2) consists of a slablike chamber 200 cm by 20 cm by 3 cm. This configuration minimizes the chamber volume (12.0 liters) and the time required to fill the clean cell with aerosol (Eq. (11)). The inside of the chamber is coated with optical-black paint, and baffles along the inner walls help collect stray light. The chamber is aluminum and weighs 50 kg (110 lb).

During operation the long dimension of the chamber is kept vertical, so that aerosol particles introduced at the top are not lost due to sedimentation. This was accomplished aboard the ship by suspending the cell from a ceiling beam with a shock-mounted universal joint. The lower mirror in the cell is continuously flushed with clean air to prevent particle deposition. To keep the aerosol at the ambient temperature and thus help preserve the optical properties, ambient air is flushed through the saddle chambers which flank the inner aerosol chamber.

The collimated laser beam is split, with the reference portion passing through a chopper and to a receiver. The other portion passes through a polarization rotator and then steps through the chamber for a total path length of 19.84 m before also passing through the chopper and to the same sensor. The beams and chopper holes are so arranged that the sensor is illuminated alternately by each beam. By this split-beam arrangement a relative transmittance measurement through the cell is obtained which is independent of variations in laser output and receiver sensitivity for frequencies smaller than the chopping rate. The 1/4-wave-plate rotator circularly polarizes the linearly polarized laser light in order that the polarization does not influence the measurement of the scattered light with the cosine sensor. The HeNe laser is from Coherent Radiation (model CR-80-4) and has an output of 4 mW, the cosine sensor (700-8B) and the S-20 photomultiplier detector assembly (2020-10) are from Gamma Scientific, and the sensor for the transmitted light is a silicon photovoltaic detector (550-2) from EG&G.

Electronic Circuitry

A phase-locked demultiplexer (Fig. 4) separates the transmitted and reference beams which, with square-wave pulses at a combined frequency of 16.67 Hz, alternately illuminate the detector. The phase-reference pulse which triggers the timers in the logic circuit is obtained from the leading edge of the reference-beam square wave. An analog switch separates the two trains of pulses into two channels, where sample-and-hold integrated circuits sample the pulse amplitude at the midpoint of each square wave and hold that amplitude long enough so that the instrumentation amplifier A_3 can difference the amplitudes to obtain ΔI. The third and fourth sample-and-hold integrated circuits stretch the pulses sufficiently to give essentially analog outputs of ΔI and I_0.

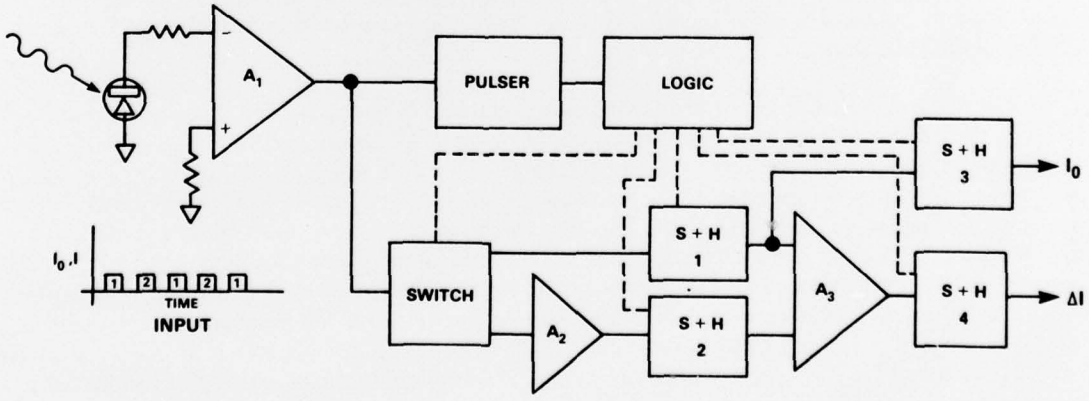

Fig. 4 — Phase-locked demultiplexer which separates the pulses of I_0 and I incident on the photosensor into analog outputs of I_0 and $\Delta I = I_0 - I$. (A indicates amplifier, and $S + H$ indicates sample and hold.)

During calibration ΔI is set to zero by adjusting the amplitude of the transmitted beam with the variable gain of A_2. The circuit can resolve changes in $\Delta I/I_0$ of 0.01%, which limit is due to noise in A_3.

The values of I_0 and ΔI, as well as the values of the scattered-light flux measured with the cosine probe and a radiometer, were sampled on different occasions at 5-s intervals for 2 min by the ship's computer, which calculated b_s and b_a according to Eqs. (2) and (9).

Aerosol and Gas Flow

The aerosol and gas flows associated with the aerosol cell are shown in the schematic in Fig. 5. The various components shown can flow aerosol concentrate through the cell, purge the cell with clean air, flush the lower mirror with clean air, fill the cell with Freon 12, and flush the Freon from the cell with clean air. During measurements of the aerosol optical properties, a volume flow V_4 of 30 l/min is drawn from the cell, of which 20 l/min is the volume flow of filtered air (V_5) used to flush the lower mirror. The remaining volume flow of 10 l/min (V_2) is drawn into the cell from the aerosol concentrator, into which 250 l/min (V_1) flows. At these flow rates it requires 2.8 min to fill the cell from a clean state to an aerosol density 90% of the final value of the aerosol concentrate (Eq. (11)). During the clean-air purge $V_4 = 0$ and $V_5 = 30$ l/min. The cosine sensor is calibrated infrequently but sufficiently to insure nondrifting electronics by filling the cell from below with Freon 12. Following calibration, the cell is flushed with clean air from above, since the density of Freon is substantially greater than that of air.

Aerosol Concentrator

The purpose of the aerosol concentrator is to increase the concentration of ambient aerosol particles a known factor over the particle-size range of importance for the wavelength of light being used in the cell. By introducing this concentrate into the cell, the atmospheric values of b and b_s are increased by a like factor. This may be accomplished in two ways: If the concentrator has a narrow particle-size bandpass, the results of multiple measurements must be added for the size range of importance. However, if the bandpass is wide enough to cover the entire range, then only one measurement is needed. It is further necessary that only small temperature and pressure changes are seen by the aerosol passing through the concentrator, since otherwise condensational growth and evaporation will change the particle size distribution.

Since the aerosol concentrator (Fig. 3) is discussed in detail in Ref. 2, only a brief description will be given here. Ambient aerosol flows at V_1 l/min into the inlet manifold 5 and along a concentric annulus formed by a solid outer cylinder 1 at rest and a porous inner cylinder 2 rotating at high speed. Suction applied at the right end of the hollow shaft 4 causes the dispersion medium to pass through the porous cylinder and into the shaft at V_3 l/min. Since the rotational velocity of the aerosol particles is comparable to that of the rotating cylinder near its surface, the particles move radially outward due to the centrifugal force, in addition to their motion to the left along the cylinder. The particles reach their highest concentration near the outlet manifold 3, where they are drawn off at V_2 l/min. With no particles exiting through the porous cylinder, the concentration increase of the aerosol particles is simply V_1/V_2, or 25 for the values of V_1 and V_2 given in the preceding section.

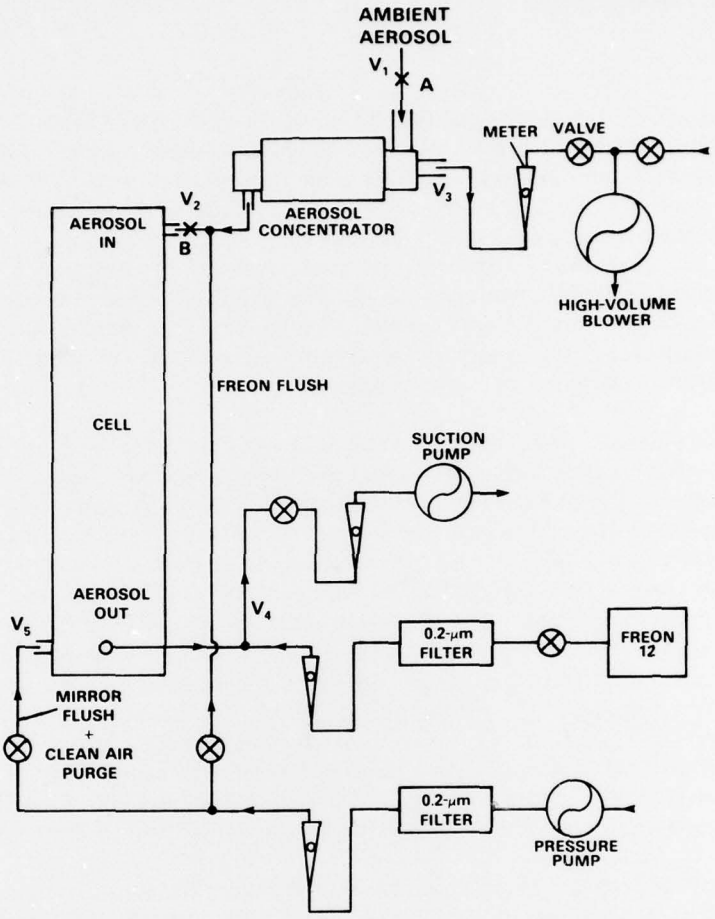

Fig. 5 — Aerosol- and gas-flow systems used with the transmission cell

The aerosol particles see only a small pressure change while passing through the concentrator. This change can be estimated from the Darcy equation for head loss in turbulent pipe flow to be less than 25 Pa (0.1 in. of $H_2 0$). The particles do not see the large pressure drop across the porous cylinder. Temperature changes are also small; the effect of aerodynamic heating in the boundary layer next to the rotating cylinder is minimized, since the slightly warmed air is drawn into the cylinder pores.

RESULTS AND DISCUSSION

Data

The data from 89 test periods during the 3 weeks of the 1977 EOMET cruise are summarized in Table 1. Each test period consisted of the following: The cell was flushed with filtered air in order to zero ΔI and to establish the background value of F. Aerosol concentrate was then sucked through the cell, which filled to a stable concentration in 6 to 8 min. After that time the average values of I_0, ΔI, and F/F_c shown in Table 1 were obtained from 24 computer samples of the sensors' outputs taken over a 2-min interval or, when the computer data were not available, from graphically averaging strip-chart records, which were taken simultaneously. Immediately following each test, the cell was flushed with filtered air, and any drift in ΔI and F was observed. In addition aerosol-size distributions were measured in the ambient as well as the concentrated aerosol.

The sample standard deviation $s(b)$ was calculated from the 24-point computer-calculated values of b for representative samples of the tests chosen as follows. The contribution to $s(b)$ was nearly all due to fluctuations in ΔI, since I_0 remained almost constant during the measurement interval. Hence the variability of $s(b)$ could be judged by dividing the tests into groups according to the amount of fluctuation in ΔI. Figure 6 shows strip-chart records of ΔI for the representative sample of each of five groups, with the samples starting from the top of the figure being from groups reflecting increasing instability. The groups represented by the top and bottom curves, which reflect the stability extremes, account for 10% of the tests. Values of $s(b)$ for the five groups were, in units of 10^{-3} m^{-1}, 0.1308, 0.1636, 0.2490, 0.2741, and 0.3157. The mean value of $s(b)$, weighted by the number of tests in each group, was 0.2281×10^{-3} m^{-1}. The Students t-distribution was applied to the values of $s(b)$ to determine the 90% confidence limits on the measurement of b: The mean limits were $\pm 0.0797 \times 10^{-3}$ m^{-1}, with $\pm 0.0457 \times 10^{-3}$ m^{-1} and $\pm 0.1102 \times 10^{-3}$ m^{-1} as the extremes. The coefficient of variation, $100s(b)/b$, is given in Table 1 for each test.

The zero of ΔI drifted a measurable amount for most tests, but the zero of F did not drift. The mean drift of ΔI was -0.021% of I_0, and the sample standard deviation of the drift was 0.240%. The drift of each test was subtracted from each measured value of ΔI. The additional uncertainty in the location of the ΔI zero is reflected in the listed values of $s(b)$, which were increased by a factor of $\sqrt{3}$.

Measured values of b_s for the aerosol concentrate are listed in Table 1. The mean sample standard deviation of b_s is 0.0157×10^{-3} m^{-1}, which gives 90% confidence limits of $\pm 0.00548 \times 10^{-3}$ m^{-1}. The values of b_s contain a systematic truncation error due to the finite field of view of the cosine sensor. This error was evaluated with Mie calculations by considering the size of the sensor and its position with respect to the multiple light passes in the cell and by using a Junge distribution with $N(r) \propto r^{-4}$, which for most tests was a reasonable approximation of the ambient-aerosol size distribution. Due to this error the values of b_s in Table 1 must be multiplied by a factor of 1.080.

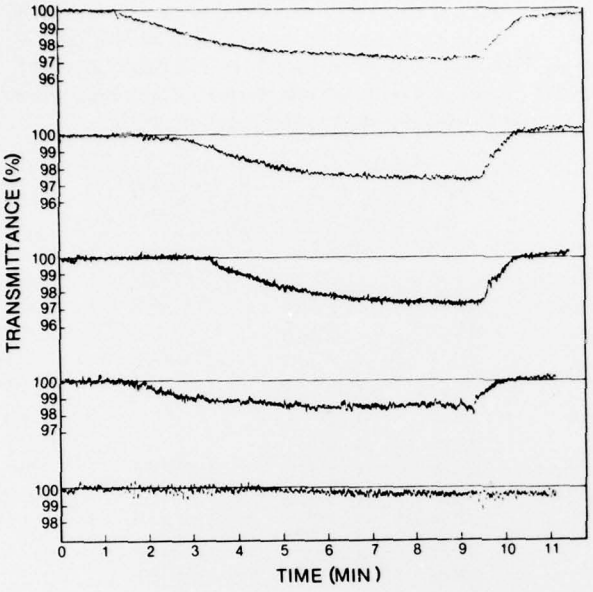

Fig. 6 — Five representative curves representing the range of stability of the transmittance measurements during the EOMET cruise. The decrease of transmittance after several minutes coincides with the filling of the cell with concentrated ambient aerosol, and the following sharp increase is the start of flushing the cell with filtered air.

Also listed in Table 1 are values of $b_s(MRI)$, which were measured in the ambient atmosphere with an *MRI* model 1560 integrating nephelometer. The ratio of $b_s/b_s(MRI)$ is shown in Fig. 7 for those tests in which aerosol generated by the ship's activities did not influence the measurements.

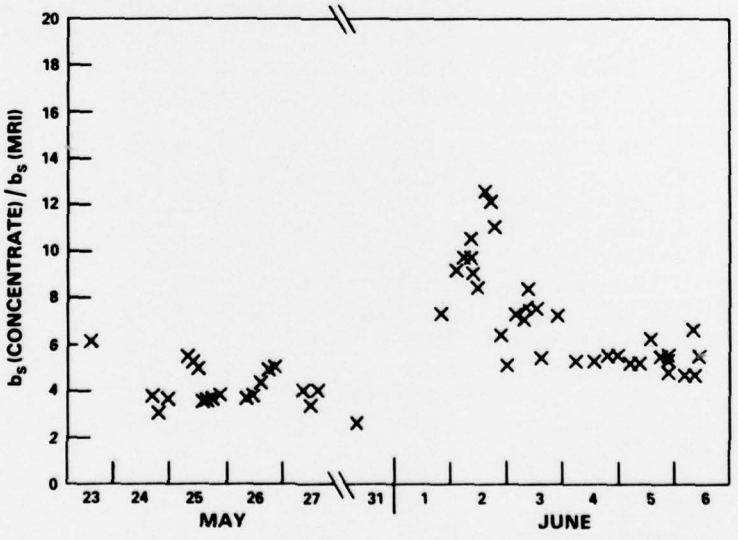

Fig. 7 — The ratio of the aerosol scattering coefficient at a wavelength of 632.8 nm for the concentrated aerosol (b_s (CONCENTRATE)) to the scattering coefficient at a quasi-photopic wavelength centered at 525.0 nm for ambient aerosol ($b_s(MRI)$)

Table 1 — Aerosol optical parameters measured during the 1977 EOMET cruise of the USNS *Hayes*. The symbols ΔI, I_0, F, F_c, b, b_s, and b_a were explained in connection with Eqs. (1) through (9) and refer to aerosol concentrate. The symbols introduced in this table are $s(b)$, which indicates the sample standard deviation, and $b_s(MRI)$, which indicates a measurement of the aerosol scattering coefficient in the ambient atmosphere taken with an *MRI* nephelometer.

Date	GMT	ΔI	I_0	F/F_c	b (10^{-3} m^{-1})	$\frac{100s(b)}{b}$	b_s (10^{-3} m^{-1})	$b_s(MRI)$ (10^{-3} m^{-1})	b_a/b
5-18*	0:30	1.08	39.0	7.96	1.42	9.2	0.830	—	0.415
5-18*	13:51	0.17	39.0	1.10	0.220	61.8	0.115	0.0227	0.478
5-18*	13:61	0.23	38.8	0.96	0.300	45.3	0.100	0.0209	0.667
5-18*	14:00	0.22	38.8	0.94	0.287	47.4	0.0980	—	0.659
5-18*	14:13	0.26	38.8	1.24	0.339	40.1	0.129	0.0155	0.619
5-19*	20:21	0.03	39.9	0.64	0.0379	35.9	0.0667	0.0163	−0.760
5-20*	13:01	0.05	39.6	0.92	0.0637	213.5	0.0960	—	−0.507
5-20*	13:34	0.15	38.8	2.00	0.195	67.1	0.209	—	−0.072
5-20*	14:20	0.10	39.6	0.91	0.127	107.1	0.0975	0.0237	0.246
5-21*	1:16	0.03	40.0	0.76	0.0378	36.0	0.0793	—	−1.098
5-22*	11:03	0.41	37.8	4.03	0.550	45.3	0.421	0.0669	0.235
5-22*	11:14	0.35	37.7	3.42	0.470	28.9	0.356	0.0654	0.240
5-22*	12:32	0.35	37.2	2.40	0.477	66.2	0.250	0.0291	0.476
5-22	17:14	0.07	35.9	0.67	0.105	300.6	0.0697	0.0184	0.336
5-23	10:48	0.05	39.0	0.92	0.0647	210.2	0.0960	0.0157	−0.484
5-24	8:07	0.51	39.0	4.68	0.664	20.5	0.488	0.120	0.265
5-24	9:56	0.13	37.6	1.16	0.161	170.3	0.122	—	0.242
5-24	12:13	0.22	39.0	1.98	0.285	96.2	0.207	—	0.274
5-24	13:53	0.08	39.0	0.68	0.103	266.1	0.0709	—	0.308
5-24	16:04	0.06	37.4	0.50	0.0809	33.9	0.0522	0.0140	0.355
5-24	18:16	−0.04	36.9	0.36	≈ 0	—	0.0375	0.0118	≈ 0
5-24	22:32	0.07	37.8	0.69	0.0934	293.5	0.0715	0.0205	0.234
5-25	8:16	0.27	39.6	2.30	0.345	72.2	0.240	0.0433	0.304
5-25	9:57	0.22	39.1	2.18	0.284	100.4	0.227	0.0418	0.201
5-25	12:17	0.19	38.2	1.84	0.251	99.2	0.192	0.0375	0.235
5-25	14:14	0.16	37.0	1.48	0.218	62.4	0.154	0.0439	0.294
5-25	16:00	0.12	37.3	1.36	0.162	153.7	0.142	0.0382	0.123
5-25	18:19	0.11	36.5	0.82	0.152	163.8	0.0855	0.0234	0.439
5-25	20:08	0.09	37.0	1.10	0.123	202.4	0.115	0.0295	0.065
5-26	9:46	0.21	36.7	2.24	0.289	86.2	0.234	0.0628	0.190
5-26	11:13	0.25	35.9	2.30	0.352	70.7	0.240	0.0607	0.318
5-26	14:28	0.29	38.5	2.94	0.381	34.3	0.307	0.0686	0.194
5-26	17:09	0.32	39.0	3.02	0.415	32.8	0.315	0.0632	0.241
5-26	19:04	0.36	38.1	2.80	0.479	28.4	0.292	0.0582	0.390
5-27	9:08	0.93	38.8	7.80	1.22	20.4	0.814	0.203	0.333
5-27	11:42	1.06	38.2	7.16	1.42	9.6	0.747	0.216	0.474
5-27	13:54	1.26	38.9	8.20	1.66	28.2	0.855	0.212	0.485
5-27*	19:52	1.06	37.5	8.42	1.45	17.2	0.878	0.157	0.394
5-27*	22:21	1.16	39.5	11.96	1.50	8.7	1.25	0.168	0.167
5-28*	6:19	0.76	39.0	9.26	0.992	13.2	0.996	0.116	0.000
5-31	8:12	0.22	39.0	1.96	0.285	87.4	0.204	0.0918	0.284
5-31*	10:20	0.56	39.1	3.64	0.727	34.2	0.380	0.0229	0.477
5-31*	12:01	0.51	38.5	4.14	0.672	47.0	0.432	0.0362	0.357
5-31*	13:57	0.38	39.0	3.60	0.494	50.4	0.375	0.0454	0.241

Table 1 (Concluded)

5-31*	16:05	0.53	38.7	5.50	0.695	39.4	0.574	0.0380	0.174
5-31*	18:19	0.35	38.8	4.70	0.457	60.0	0.490	0.0508	−0.072
5-31*	19:40	0.42	38.6	5.20	0.552	49.7	0.542	0.0462	0.018
5-31*	21:53	0.25	38.7	3.20	0.327	76.1	0.334	0.0389	−0.021
6-1*	4:11	0.52	39.3	6.20	0.671	37.1	0.647	0.0987	0.065
6-1*	6:21	1.06	39.2	10.40	1.38	18.0	1.08	0.101	0.268
6-1*	9:27	0.24	38.4	3.81	0.316	43.0	0.313	0.0397	0.010
6-1*	12:04	1.00	38.4	10.20	1.33	20.6	1.06	0.0523	0.203
6-1*	14:08	0.83	38.5	8.40	1.10	12.4	0.876	0.0504	0.204
6-1*	14:45	1.09	38.9	10.26	1.43	9.5	1.07	0.0468	0.252
6-1	19:45	0.35	37.6	3.80	0.471	58.2	0.396	0.0537	0.159
6-2	4:19	0.49	37.5	6.00	0.663	37.6	0.626	0.0655	0.056
6-2	5:23	0.56	37.0	7.38	0.769	32.3	0.759	0.0771	0.013
6-2	6:25	0.52	37.1	6.80	0.712	35.0	0.709	0.0724	0.000
6-2	8:12	0.60	37.0	7.08	0.741	33.6	0.738	0.0706	0.004
6-2	10:07	0.55	37.7	6.28	0.741	37.0	0.655	0.0710	0.116
6-2	11:58	0.49	36.2	6.00	0.687	36.2	0.626	0.0735	0.089
6-2	14:04	0.60	36.0	7.40	0.847	29.4	0.772	0.0613	0.089
6-2	16.25	0.55	36.2	6.56	0.772	35.5	0.684	0.0553	0.114
6-2	18:04	0.53	36.3	6.06	0.741	37.0	0.632	0.0571	0.147
6-2	20:33	0.55	38.5	5.46	0.725	37.8	0.569	0.0899	0.215
6-2	22:22	0.57	37.4	5.90	0.774	32.2	0.615	0.0919	0.205
6-2	23:11	0.15	37.4	1.70	0.203	135.0	0.177	0.0344	0.128
6-3	4:10	0.61	38.6	7.20	0.803	34.1	0.751	0.101	0.065
6-3	6:13	0.60	38.3	6.40	0.796	35.6	0.668	0.0865	0.161
6-3	7:56	0.57	37.7	6.10	0.768	17.7	0.636	0.0820	0.171
6-3	10:02	1.10	38.3	10.76	1.47	16.9	1.12	0.133	0.236
6-3	12:02	0.92	38.1	9.40	1.23	10.6	0.980	0.129	0.205
6-3	14:03	0.31	38.1	2.72	0.412	33.0	0.284	0.0509	0.311
6-3	21:21	0.25	37.4	2.96	0.338	73.7	0.352	0.0485	−0.041
6-4	8:21	0.25	36.9	2.82	0.343	72.6	0.294	0.0550	0.143
6-4	14:16	0.32	35.7	3.58	0.454	54.8	0.373	0,0697	0.178
6-4	20:19	0.67	35.2	7.44	0.696	14.0	0.776	0.140	0.199
6-5	0:14	0.64	38.0	7.56	0.856	15.9	0.789	0.140	0.078
6-5	4:35	0.52	39.1	4.90	0.675	36.9	0.511	0.0970	0.243
6-5	8:14	0.66	39.9	6.44	0.841	16.2	0.672	0.125	0.201
6-5	14:28	0.58	37.5	4.78	0.786	17.3	0.688	0.109	0.125
6-5	18:22	0.47	36.9	5.06	0.646	42.4	0.528	0.0970	0.183
6-5	20:10	0.50	37.0	4.74	0.686	40.0	0.494	0.0987	0.280
6-5	20:35	0.68	36.9	6.26	0.938	29.2	0.653	0.123	0.304
6-5	20:54	0.67	37.1	6.24	0.9191	29.8	0.651	0.118	0.292
6-5	23:25	0.24	36.3	2.20	0.334	82.1	0.229	0.0491	0.314
6-6	4:14	0.38	37.0	3.46	0.520	52.7	0.361	0.0808	0.306
6-6	6:31	0.40	37.3	3.50	0.544	50.4	0.365	0.0817	0.329
6-6	10:10	0.70	37.1	5.28	0.960	25.9	0.551	—	0.426

*Measurement influenced by ship-generated aerosols.

The last column of Table 1 lists the fraction b_a/b of the light extinction at 632.8 nm due to the absorption by the aerosol particles in the concentrate. Figure 8 shows the values $b_a/b = 1 - \omega_0$, where ω_0 is the bulk single-scattering albedo, for the tests free of the ship's influence. The truncation error is included in the Fig. 8 data.

During each test the ambient-aerosol size distribution was measured at point *A* of the system (Fig. 5) and the distribution in the concentrate was measured at point *B*. Figure 9 gives as a function of particle size the average ratio between the measurement at *B* and the measurement at *A* as the factor by which the ambient concentration was increased by the aerosol concentrator. Data for two concentrator rpm values are given; 8000 rpm was used during the tests prior to 1 June, and 10,000 rpm was used thereafter.

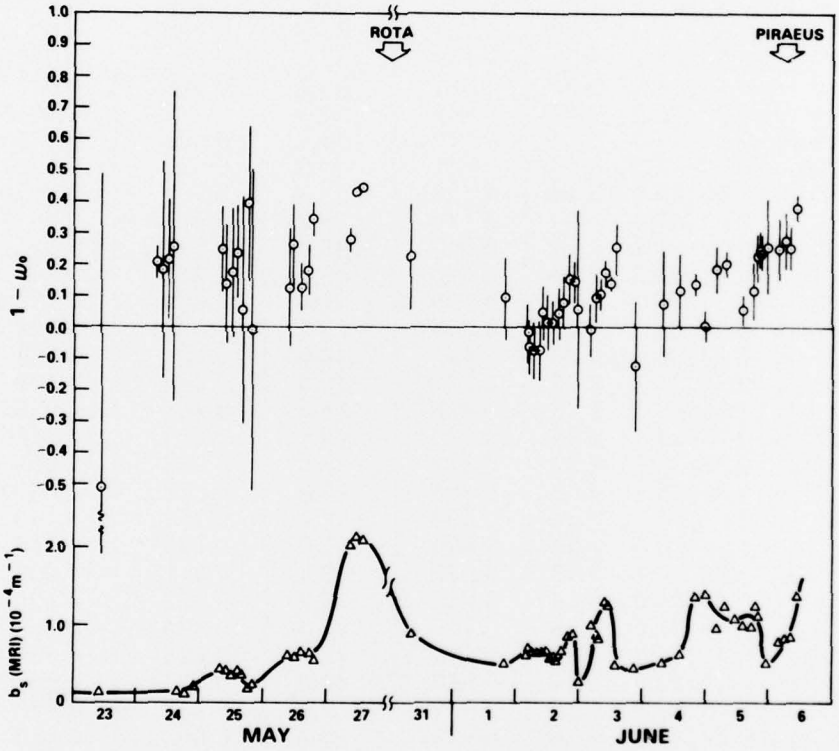

Fig. 8 — Bulk single-scattering albedo ω_0 (where $1 - \omega_0 = b_a/b$) for the laser wavelength of 632.8 nm (upper data); lines extending above and below each point are 80% confidence intervals. The lower curve is the aerosol scattering coefficient from the *MRI* integrating nephelometer, model 1560.

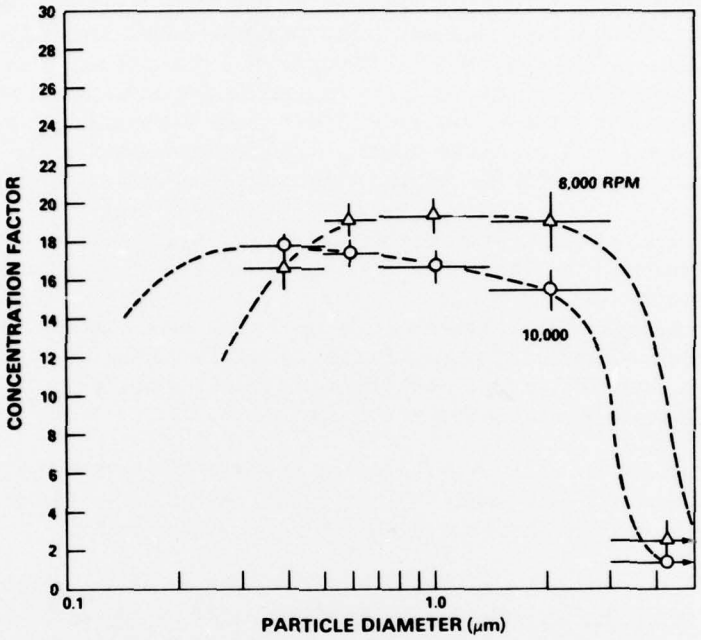

Fig. 9 — Increase in the particle concentration over ambient values at the output of the aerosol concentrator for two instrument rpm values. The horizontal lines show the width of the sizing channels in the Royco particle counter. The vertical lines are 90% confidence intervals.

System Performance

Transmittance Measurements

The mean resolution limit of the cell transmittance measurements during the cruise is ±0.16%, under the assumption that the resolution limit is given by the mean 90% confidence limits ($\pm 0.0797 \times 10^{-3}$ m^{-1}) of the measurements of b, each of which entailed 24 point samples over a 2-min interval. This resolution reflects some deterioration of the accuracy found previously in the laboratory. The reasons for the difference are as follows:

• The major cause of error was the drift of the ΔI zero between the time that concentrate was first introduced into the cell and after the cell was flushed with clean air. The cause of the drift was slow beam wander on the transmitted-light sensor due to thermal flexing of the cell. This was the case whenever the ambient and concentrate temperatures differed from the temperature of the cell. Such thermal flexing occurred on numerous occations, since the location of the cell on the ship, just under the metal deck near the bow in one of the ship's twin hulls, caused temperature differences as great as ±10°C, which could not be entirely eliminated with the saddle conditioning chambers on the cell.

• Another cause of error, much less on the average but large on occasions, was the wave-induced motion of the ship. Under the roughest sea conditions experienced (seas of 3 to 4.5 m), longitudinal stresses on the cell, caused by accelerations approaching ±1.0 g, resulted in slight warpage of the cell and again beam wander on the sensor. The lowest curve in Fig. 6 was obtained during the roughest weather, and the effect of wave trains passing by the ship is clearly seen. Higher frequency vibrations from the ship's machinery were filtered out by the shock-mounted suspension of the cell.

• The higher frequency noise in ΔI, as seen in the middle curves of Fig. 6, was due to scintillation of the beam. This source of error, caused by turbulence in the cell, was largest for large temperature differences between the cell and the ambient air.

• A small source of error was the instability of the line voltage, which after improvement changed up to 5%, depending on the local load. The stability of the laser and the demultiplexer proved adequate, and particle deposition on the mirrors in the cell was insignificant, as revealed by inspection.

In summary, the resolution limit of the transmittance measurements reflects almost entirely mechanical problems in the cell design. The resolution limit could easily be bettered by a factor of 10 with an improved cell.

Scattering Measurements

The noise in the measurement of b_s was small, and the zero drift was insignificant. Of greater importance were possible sources of systematic error. The truncation error, calculated as was described in the data subsection for a typical particle size distribution, will fluctuate somewhat about the given correction, since it is a function of the changing ambient-aerosol size distribution. Another possible source of error is the imperfect cosine response of the radiometer. Although the manufacturer shows a precise cosine response for parallel incident light, some deviations will exist for our application, since the scattered light from the beams in the cell is only approximately parallel. A final source of uncertainty is the value of b_{sc} for Freon 12, for which an error estimate was not published.

Concentrator Performance

Figure 9 shows that the width of the particle-size bandpass of the concentrator is slightly greater than one order of magnitude. This width should have been sufficient to properly scale up the values of b and b_s in the cell for the cases in which the centrifuge operated at 10,000 rpm, since it is known that most of the attenuation of light with a wavelength of 632.8 nm is due to particles between about 0.1 and 1.0 μm in diameter. To judge this con-

clusion, the data in Fig. 7 may be used. These data, most of which reflect a strong continental influence, show $b_s/b_s(MRI)$ has an average value of 5.7. Since in the cell b_s was measured at a wavelength of 632.8 nm and the *MRI* nephelometer operates at 525.0 nm with a quasi-photopic light source [10], it is necessary to wavelength correct the factor of 5.7 before it is compared to the concentration in Fig. 9. Duntley et al. [11] made b_s measurements at nearly the same wavelength interval: A quasi-photopic source at 550.0 nm and a narrow red filter centered at 664.0 were used during aircraft measurements in Europe. A 200-point average of b_s values measured in the atmospheric boundary layer during seven flights gave a green-to-red scattering ratio of 3.92. The product of 5.7 × 3.92 is reasonably close to the enhancement factor in Fig. 9 to support the conclusion that the bandpass in Fig. 9 is sufficient to properly scale up the values of b and b_s. A precise determination of the relationship between the values of b and b_s measured in the cell and those in the atmosphere is not possible without additional Mie calculations. However, a good guess is that the chamber measurements divided by the mean concentration factor are within 10% of the ambient values.

Transmittance Measurements in the Infrared

A rough estimate is possible of how the present approach applies to the infrared. Since the extinction due to aerosols generally decreases with increasing wavelength of light, the measurement error will become a larger fraction of the measured b. The increase in the error is equal to the ratio of extinction coefficient at 632.8 nm to that in the infrared for the same aerosol, under the assumption that the same resolution limit measured in this experiment applies to the cell instrumented with the infrared source and optics. As an example, McClatchey et al. [12] give a ratio of 13.7 for the extinction coefficient at 632.8 nm and at 10.6 μm (CO_2 laser). This means that, for the infrared measurement, atmospheres with greater particle loading are required to obtain the same measurement error given by the 632.8-nm measurement. For instance, the error for a value of b equivalent to 100 km visibility at 632.8 nm is the same as for a value of b measured with the CO_2 laser in an atmosphere with a 7.3-km visibility at 632.8 nm. From these figures it appears feasible to measure infrared transmittance in the hazier atmospheres with the present approach.

Uncertainties not included in the preceding estimate are cell-induced errors and infrared-light-source and detector stability. Also the particle-size bandpass shown in Fig. 9 would probably not be adequate for the long-wavelength infrared, since larger particle sizes are more important. However, it appears possible to shift the bandpass to larger particle sizes by operating the concentrator in a different mode. These uncertainties are best resolved by modifying the present system for measurements in the infrared.

CONCLUSIONS

The use of the portable transmission cell and the aerosol concentrator during the 1977 EOMET cruise of the USNS *Hayes* led to the following conclusions:

- It is feasible to measure laser-attenuation onboard a ship at sea with a portable transmission cell used in conjunction with an aerosol concentrator. The resolution of the aerosol-optical-depth measurements in the cell for λ = 632.8 nm had a mean value of $\pm 1.58 \times 10^{-3}$. The concentrate gives an effective pathlength in the cell of about 300 m.

- The resolution is limited by mechanical weaknesses in the cell. Flexing of the cell due to ambient-and-cell temperature differences and longitudinal stresses from wave-induced ship motion cause beam wander on the transmitted-light sensor.

- It may be feasible with the present technique to measure infrared transmittances for wavelengths as long as 10.6 μm under hazy atmospheric conditions.

- An improved cell could better the resolution by a factor of 10 or more. Thus the concentrator could become an unnecessary accessory.

- The reciprocal integrating nephelometer used on the cell is a practical alternative to the standard nephelometer.

- The aerosol concentrator produces a particle-size bandpass which scales up the values of the extinction and scattering coefficients measured in the cell from values in the atmosphere with an uncertainty of about 10%.

- The combination of extinction and scattering measurements in the same aerosol provides a unique means of measuring the particles absorption coefficient in real time. If in addition the particles' size distribution is measured, Mie calculations will give the complex index of refraction of the particles more accurately than given by other techniques.

RECOMMENDATIONS

Recommendations for future action are as follows:

- The successful demonstration of the shipboard use of the portable transmission cell for a visible laser wavelength calls for the testing of this technique with infrared sources and optics, since the potential usefulness of this technique is greatest for those wavelengths of light.

- Additional evaluation of the concentrator is needed in order that the relationship between the particle-size bandpass and the operating mode of the instrument are well established.

- The reciprocal type of nephelometer, the potential of which has been overlooked, should be exploited. A visibility meter responsive from clear air to fog conditions appears practical. Its development for measuring the aerosol scattering coefficient in the infrared, which no devices presently do, likewise appears feasible.

ACKNOWLEDGMENTS

The data for $b_s(MRI)$ was collected by Dr. James Fitzgerald. Appreciation is expressed to Mr. Robert Stilling for his fabrication of the cell and his able assistance during the EOMET cruise.

REFERENCES

1. R.W. Fenn, "Optical Properties of Aerosols," in *Handbook on Aerosols*, R. Dennis, editor, U.S. Energy Research and Development Administration, TID-26608, 1976.
2. H.E. Gerber, "Centrifugal Concentration of Aerosol Particles," submitted to *Aerosol Sci*, 1978.
3. R.J. Charlson, N.C. Ahlquist, H. Selvidge, and P.B. MacCready, "Monotoring of Atmospheric Aerosol Parameters with the Integrating Nephelometer," *J. Air Pollution Control Assoc.* 19, 937-942 (1969).
4. R.E. Weiss, A.P. Waggoner, R.J. Charlson, D.L. Thorsell, J.S. Hall, and L.A. Riley, "Studies of the Optical, Physical, and Chemical Properties of Light Absorbing Aerosols," preprints for Conference on Carbonaceous Aerosols, Mar. 20-22, 1978, Berkely, Calif.
5. R.G. Beuttell and A.W. Brewer, "Instruments for the Measurement of the Visual Range," *J. Sci. Instr.* 26, 357-359 (1949).
6. V.E. Zuev, M.V. Kabanov, and B.A. Savel'ev, "The Limits of Applicability of the Bouguer Law in Scattering Media for Collimated Light Beams," (English trans.), *Izv. Atm. and Oceanic Phys.* 3, 724-732 (1967) and (English trans.) *Atm. and Oceanic Phys.* 3, 414-418 (1967).
7. R.C. Sepucha and D. Mann, "Aerosol Attenuation In The 2-4 μm Region," Rome Air Development Center, Technical Report RADC-TR-75-113, 1975.
8. D.S. Ensor, R.J. Charlson, N.C. Ahlquist, K.T. Whitby, R.B. Husar, and B.Y.H. Liu, "Multiwavelength Nephelometer Measurements in Los Angeles Smog Aerosol, I," *J. Colloid and Interface Sci* 39, 242-251 (1972).
9. C.N. Davies, "Deposition from Moving Aerosols," pp 393-446 in *Aerosol Science*, C.N. Davies, editor, Academic Press, New York, 1966.
10. A.P. Waggoner, personal communication, 1978.
11. S.Q. Duntley, R.W. Johnson, and J.I. Gordon, "Airborne Measurements of Atmospheric Volume Scattering Coefficients In Northern Europe, Spring 1976," Scripps Institute of Oceanography, San Diego, Ref. 77-8, AFGL-TR-77-0078, 1977.
12. R.A. McClatchey, R.W. Fenn, J.E.A. Selby, F.E. Volz, and J.S. Garing, "Optical Properties Of The Atmosphere (Third Edition)," Air Force Cambridge Research Laboratories, Environmental Research Paper 411, 1972.